LLNL-JRNL-829009

LAWRENCE
LIVERMORE
NATIONAL
LABORATORY

# Volatile Products of the Autoxidation of Poly(ethylenimine) in CO2 Sorbents

J. Racicot, S. Li, A. Clabaugh, C. Hertz, S. A. Akhade, E. Ping, S. H. Pang, M. Sakwa-Novak

November 8, 2021

Journal of Physical Chemistry C

## Disclaimer

LLNL-JRNL-829009

# Volatile Products of the Autoxidation of Poly(ethylenimine) in $CO_2$ Sorbents

*Joan Racicot,[1] Sichi Li,[2] Abigayle Clabaugh,[1] Cassandra Hertz,[1] Sneha A. Akhade,[2] Eric W. Ping,[1] Simon H. Pang,[2] Miles A. Sakwa-Novak[1]**

[1]Global Thermostat LLC, 10275 E 106th Ave., Brighton, CO 80601, United States

[2] Materials Science Division, Lawrence Livermore National Laboratory, 7000 East Ave, Livermore, CA 94550, United States

*miles@globalthermostat.com

**ABSTRACT:**

Poly(ethyleneimine) (PEI) based $CO_2$ sorbents are a promising material class for use in $CO_2$ capture applications, particularly Direct Air Capture (DAC), due to their high amine content and $CO_2$ capacities. Sorbent lifetime is a key uncertainty in the deployment of these materials in such applications, as they oxidize under conditions relevant to candidate DAC process cycles. Here, we utilize TGA-DSC-FTIR to characterize the nature, rate, and quantity of volatile species formed from the oxidation of PEI when supported on a mesoporous $Al_2O_3$. We show that $NH_3$, $CO_2$, and $H_2O$ are primary volatile species formed from PEI oxidation, and that their production rate matches the overall oxidation rate as measured via heat flow from a DSC. We show that the total quantity of $NH_3$ evolved is consistent with terminal primary amines being cleaved from the polymer chain, and that approximately one hydrogen atom per PEI repeat unit reacts to form $H_2O$ during the reaction. Finally, metadynamics and quantum chemical simulations performed on a simplified system are used to highlight the likely importance of radicals in the elementary reactions that comprise the oxidation reaction set. The findings here represent the first characterization of the volatile products from the oxidation of PEI in $CO_2$ sorbents, and lead to a greater understanding of the mechanisms behind the oxidative degradation of these materials.

**Keywords**: Direct Air Capture, Supported Amine Adsorbent, Polymer Oxidation, Poly(ethylenimine), Sorbent Lifetime

**Synopsis:** The volatile oxidation products of a poly(ethylenimine) based Direct Air Capture sorbent are characterized for the first time and analyzed in the context of their practical and fundamental implications.

**TOC Graphic:**

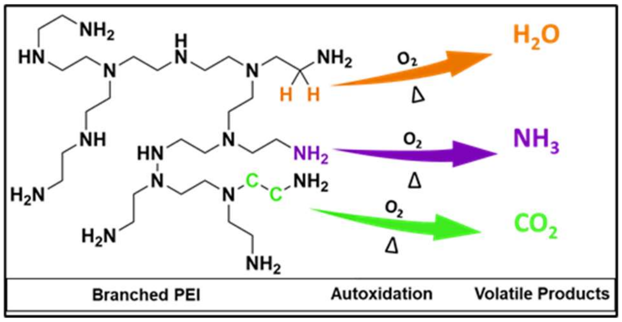

NH2
HN
N
H
N
N
NH2
H H
O2
Δ
H2O
NH
HN
N
NH2
O2
Δ
NH3
H2N
N
N
C
C
NH2
O2
Δ
CO2
H2N
NH2
Branched PEI
Autoxidation
Volatile Products

## Introduction

Poly(ethylenimine) (PEI) based sorbents are promising materials for $CO_2$ capture applications such as Post-Combustion Flue Gas Capture and Direct Air Capture (DAC).[1–5] These applications involve separating $CO_2$ from gas streams at concentrations ranging from ~5-15% (flue gas) to 400 ppm (air). In particular, PEI and similar amine molecules are essential for the ultra-dilute nature of DAC processes where a chemisorptive interaction is advantageous.[1,5] PEI can be incorporated into porous support materials such as mesoporous metal oxides, MOFs, or other material families to form composite sorbents that selectively bind $CO_2$ at these dilute concentrations over $N_2$, $O_2$, and other gaseous species, including in the presence of humidity.[6–10] These sorbent materials are proposed to be used in a variety of process designs, such as temperature vacuum swing adsorption,[11] steam stripping,[12,13] pressure swing adsorption,[14] amongst others. Further, the sorbents have been proposed to be formed into a variety of form factors such as powders,[15] pellets, honeycomb monoliths,[16] hollow fibers,[17] and others to create advanced sorbent contactor designs.

One drawback to the use of amine-based sorbents is their susceptibility to oxidative degradation.[18–20] Like many commercial organic and polymeric materials, PEI will slowly oxidize even at ambient conditions and eventually lose its capacity to adsorb $CO_2$. Sorbents deployed for use in $CO_2$ capture applications will be exposed to $O_2$-containing gases during various steps during their cycle, but also during manufacturing, shipping, storage, and handling. Therefore, it is important to develop a comprehensive understanding of the rates and mechanisms by which they oxidize to support their commercial use.

The oxidative degradation of solid amine sorbents has been studied and reported by various researchers and recently reviewed.[21] In many cases, accelerated methods are used to study the oxidation of the material by exposure to higher temperatures and/or greater $O_2$ concentrations than material would see in a typical process. Significant effort has been allocated to studying the reaction products of the oxidative degradation of PEI and other similar molecules.[19,22–26] FTIR experiments performed on the sorbent material either before and after, or during, exposure to accelerated oxidative conditions have shown a large peak in the 1690-1650 $cm^{-1}$ range that has been attributed to carbonyl and imine species that form on the PEI backbone.[22,24,27,28] Ex-situ $^{1}H$ and $^{13}C$ NMR following similarly accelerated treatments have helped in further specifying structures of particular multi-repeat unit oxidized PEI fragments.[20,29] 2D NMR of oxidized PEI and grafted amines extracted from their support material gave greater resolution to these products, and showed several specific carbonyl- and imine-containing fragments that form.[23,30] Imine and carbonyl species both contain double bonds that are not initially present on the material, and therefore require loss of hydrogen. Early literature reports on the oxidation of supported amines posed that primary amines were more stable than secondary amines.[20,27] However, subsequent publications provided examples to the contrary, [26,31] highlighting the complexity of the reactions occurring.

Important strategies have been demonstrated to mitigate oxidation through novel amine structures,[26,27,31–34] chemical functionalization,[35–37] interaction with the support,[38] and the use of scavengers and additives.[28,35,39] However, developing a deeper understanding of the oxidation mechanisms of the base PEI molecule remains important to support its deployment in commercial sorbents and to develop further targeted strategies for improvement.

Recently we have developed a method for measuring the oxidation rate of PEI in $CO_2$ sorbents by differential scanning calorimetry (DSC), and have used this method to develop an oxidation rate law.[40] This study revealed over the course of the reaction, ~15-20% of the mass of PEI is lost and further that a disproportionate and systematic amount of N and H species are lost relative to C in the polymer structure over this period. These findings show that oxidation products evolving to the vapor phase are significant in the reaction. Volatile products are known to form during the oxidation of aqueous amines in solvent-based $CO_2$ capture processes.[41–43] However, there have been no reports to date on the volatile products that form during the oxidation of PEI to account for this mass that is lost.

In this contribution, we address this by probing the vapor phase species formed during the oxidation of PEI via TGA-DSC-FTIR experiments. Using this method, we show that $NH_3$, $CO_2$, and $H_2O$ are primary volatile species formed during the reaction, quantify their production rates in relation to the reaction rate, and propose potential reaction types to explain their formation.

## Materials and Methods

### *Sorbent Preparation*

The materials used in this study were similar to those used in previous work.[40] Sorbents were comprised of lower molecular weight, branched poly(ethylenimine) (PEI) (Sigma-Aldrich, part number 408719), and commercially sourced mesoporous $\gamma$-$Al_2O_3$. The sorbent was prepared by impregnating the $Al_2O_3$ with PEI, targeting a 70% pore fill of the $Al_2O_3$ mesopore volume. The $Al_2O_3$ powder was dried overnight at 100 °C before impregnation. Approximately 6.9 grams of PEI was added to 500 mL of DI water and stirred until fully dissolved. Then 10.5 grams of the dried $Al_2O_3$ was added to the solution and allowed to stir overnight at room temperature to ensure all the $Al_2O_3$ was dispersed and properly mixed with the PEI solution. The water was removed by rotary evaporation at 50 °C and the resulting sorbent was then dried in a vacuum oven at 100 °C for 10 hours to evaporate any remaining solvent. The dried sorbent was verified for its target pore fill using $N_2$ physisorption and thermogravimetric analysis. The method produced sorbent with a measured PEI pore fill of 69%.

*Material Characterization*

N$_2$ physisorption was performed on a Micromeritics TriStar II 3020 at 77 K using ~100 mg of the sorbent. Prior to analysis, the sample was degassed under vacuum for 10 hours at 100 °C. The pore volume of the sample was determined from the maximum value when the relative pressure ($P/P_0$) is approximately 0.99. The pore fill of the sorbent was calculated from the difference in pore volume of the bare $Al_2O_3$ powder compared to the sample's pore volume on a per gram of $Al_2O_3$ basis.

Thermogravimetric analysis (TGA) was used to calculate organic content of the sorbent. Organic combustion was performed on a Netzsch (STA 449 F3 Jupiter) under $N_2$-diluted air. The sample was heated to 900 °C with a ramp rate of 10 °C/min. The organic content was taken as the mass loss between 175 °C and 900 °C, with the mass remaining at the end of the experiment comprising the $Al_2O_3$ support. The pore fill of the sorbent was calculated by dividing the loaded PEI volume by the pore volume of the $Al_2O_3$ support.

Elemental Analysis. CHN analysis was performed on an Elementar Unicube. Samples were dried under vacuum at 100 °C for 10 h to avoid $H_2O$ and $CO_2$ adsorption on the surface prior to analysis. 5 mg samples were run in triplicate to estimate the error in the measurement.

*TGA-DSC-FTIR Oxidation Experiments*

The TGA-DSC-FTIR apparatus consisted of a Netzsch STA 449 F3 Jupiter TGA/DSC and a Thermo Scientific Nicolet iS50 FT-IR spectrometer equipped with a TGA/IR Accessory gas cell. The furnace and gas cell were coupled through a heated (300 °C) and insulated stainless steel transfer line. The FTIR interferometer was continuously purged with nitrogen. The gas cell was purged with nitrogen before the start of each experiment while a series of basis vectors were collected to be used as the background. Spectra were collected every 30 seconds in the range of

400-4000 $cm^{-1}$ at 4 $cm^{-1}$ resolution. The exhaust of the FTIR gas cell was further connected to a LiCOR 850a quantitative $CO_2$/$H_2O$ analyzer for quantitative $CO_2$ and $H_2O$ analysis. A photograph and schematic of the setup is given in Figures S2 and S3, respectively.

Isothermal oxidation experiments were conducted on approximately 100 mg of the sorbent material in a 0.19 mL platinum pan with a pierced lid. The temperature was ramped at 5 °C/min to 100 °C under $N_2$ to remove water and $CO_2$ from the sample. The temperature was held at 100 °C for 300 minutes before ramping again under $N_2$ to the designated temperature (125, 137.5, or 150 °C) at 5 °C/min. The temperature was held under $N_2$ for 180 minutes before switching to a constant 110 mL/min flow of gas containing $O_2$ at concentrations of 5% or 17% balanced with $N_2$. This isothermal, oxidative environment was maintained for a specific amount of time to measure the heat flow and mass loss. To prevent any further oxidation, the sample was then cooled under $N_2$ to room temperature. During these experiments, for each oxidative condition, the DSC measures the incremental heat flux which increases, levels out, and then decreases to zero. The oxidation is considered complete when the integrated heat flow over 10 minutes changes less than ±0.01% of the total integrated heat. For partial oxidation experiments, the method was terminated before completion of the oxidation reaction.

*Data Treatment and Workup*

<u>TGA/DSC Experiments.</u> DSC data were converted from the base unit of mW/mg sorbent to W/gPEI using the PEI loading measured by TGA burnoff described above. DSC data were corrected for drift by applying an offset, determined by the heat flow value when the DSC curve approached a horizontal line. The total heat evolved was calculated by integrating heat flow over time. The extent of oxidation from DSC was calculated by dividing the integral heat flow curve

by the total heat evolved. A more detailed description of the DSC heat balance and data treatment is given in our previous work.[40]

TGA-IR Experiments. The amount of $NH_3$ evolved during oxidation experiments was tracked by the FTIR peak area between 987 $cm^{-1}$ and 918 $cm^{-1}$ and utilizing a calibration curve. The calibration curve is shown in Figure S4. The calibration curve was created utilizing $NH_3$ gas standards purchased from Airgas in certified cylinders. Gas at three concentrations from the cylinders (10 ppm, 100 ppm, and 1000 ppm) was purged through the FTIR gas cell at a flow rate of 110 mL/min (the same overall flow rate as used in the oxidation experiments). The integral intensities between 987 $cm^{-1}$ and 918 $cm^{-1}$ were calculated for each concentration. A linear relationship between absorbance and $NH_3$ concentration was observed (Figure S4) and the Beer-Lambert Law was used to calculate the concentration of $NH_3$ in mol/L for samples. The extent of oxidation from this method was calculated by integrating the concentration of $NH_3$ over time and normalizing by the total amount of $NH_3$ evolved during the experiment; this is the same methodology as is used for the DSC extent of oxidation calculation.

*Comment Regarding Laboratory Altitude*

Our laboratories are located in the greater Denver, CO, USA area with an altitude of ~5000 ft (~1500 m). This altitude sets zero-gauge pressure at an absolute pressure of ~0.845 bara; all experiments reported here were performed at close to zero-gauge pressure and at the concentrations noted. Experiments performed at altitudes closer to sea level, where the gauge pressure is closer to 1 bara, will result in higher partial pressures of gaseous species.

Modeling Methods:

Ab initio molecular dynamics (AIMD) and metadynamics simulations were performed with the Vienna ab initio simulation package (VASP), version 5.4.4,44 using the projector augmented wave treatment of core-valence interactions[45,46] with the Perdew-Burke-Ernzerhof (PBE) generalized gradient approximation[47] for the exchange-correlation energy. A 15 Å × 15 Å × 15 Å cubic supercell was used to isolate each molecule from its periodic images and the Brillouin zone was sampled at the Γ-point only. Triethylenetetramine (TETA) was used as a simplified model compound representative of chemical motifs present in PEI. 5 ps of NVT AIMD simulations at 373 K were run for TETA-derived reactants, intermediates, and products and low-energy snapshots along the trajectories were quenched to 0 K to obtain stable optimized geometries. PBE-optimized structures were reoptimized with Becke-3 Parameter-Lee-Yang-Parr (B3LYP) functional[48,49] and 6-311+G(d,p) basis set using Gaussian09.[50] Vibrational frequencies were computed at the same level of theory for thermal corrections of energies and entropies. Single-point Coupled Cluster single-double and perturbative triple (CCSD(t)) calculations with basis set 6-31G(d) were performed to further refine the energies of B3LYP-optimized structures using NWCHEM[51] with wavefunction computed based on either closed-shell restricted Hartree-Fock (RHF) or restricted open-shell Hartree-Fock (ROHF) methods.

Metadynamics simulations[52] were performed to determine the free energy barriers of $NH_3$ formation reactions. The coordination numbers between alpha-C and terminal-N, and terminal N and all H atoms were selected as the two collective variables (CV) to drive the occurrence of C-N bond cleavage and N-H bond formation. Simulations were terminated when CVs crossed from the reaction basin into the target product basin following a previously reported protocol.[53] The free energy barrier was computed by summing up the amount of bias potentials accumulated in the reactant basin.

**Results & Discussion**

It has recently been shown that a substantial and systematic amount of mass is lost from poly(ethylenimine) (PEI) based $CO_2$ sorbents during their oxidation. Specifically, our previous work established that from start to finish in an oxidation reaction, PEI loses ~15-20% of its mass due to the formation of volatile reaction products and that a systematic change in the elemental composition of the remaining PEI occurs. Here, we have utilized a TGA-DSC-FTIR setup to track the evolution of volatile products of the autoxidation of PEI in a $CO_2$ sorbent *in-situ*. The sorbent is a PEI impregnated mesoporous $\gamma$-$Al_2O_3$ material, the same as used in our previous work. The support and sorbent properties are provided in Table S1 of the Supplementary Information (SI). $N_2$ physisorption isotherms for the support and sorbent are given in Figure S1. A photograph and schematic of the experimental setup utilized in this study is shown in Figures S2 and S3, respectively. Briefly, samples are exposed to a controlled thermooxidative environment isothermally in a TGA/DSC. A heated transfer line connects the exhaust of the TGA to the inlet of an FTIR gas analysis cell. The exhaust of the FTIR cell is further connected to the inlet of a LiCOR 850a quantitative $CO_2$/$H_2O$ analyzer before it is finally exhausted. In this way, the mass loss, heat flow, and volatile gas species produced during the reaction can all be tracked *in-situ*.

Our previous work established that heat flow measured from the DSC can be converted to the extent of reaction for the autoxidation reaction of PEI. This allows for experiments conducted at different conditions to be evaluated at the same point in the reaction, rather than at the same point in time. Figure 1 shows baseline corrected FTIR spectra for the effluent gas from isothermal exposures at 150 °C at timepoints corresponding to 0%, 33%, 66%, and 99% of extent of reaction under 17% $O_2$ and 0% $O_2$ (purely thermal) conditions. Similar spectra for the 125 °C and 137.5 °C experiments are shown in Figures S5 and S6 of the SI; data for the 150 °C experiments are shown here as the peaks are most intense and easy to observe. The figure is annotated with assignments to species assigned to the particular bands.

Figure 1 shows several important features. First, spectra resulting from the oxidative conditions show the emergence of several peaks, while those from the purely thermal conditions remain relatively unchanged. Peaks emerge in the oxidative effluent at 4000-3500 cm$^{-1}$, 3333 cm$^{-1}$, 2780-3000 cm$^{-1}$, 2360 cm$^{-1}$, 2330 cm$^{-1}$, 1875-1275 cm$^{-1}$, 964, and 932 cm$^{-1}$. Figure 1 shows the assignments made to each of these groups. Briefly, the peak at 3333 cm$^{-1}$ is attributed to the N-H stretch in $NH_3$ and the peaks at 964 cm$^{-1}$ and 932 cm$^{-1}$ are N-H bending in $NH_3$. Peaks in the 4000-3500 region, 1875, and 1275 are associated with $H_2O$. Peaks at 2360 and 2330 are associated with $CO_2$. Finally, peaks in the 2780-3000 range are associated with C-H stretching.

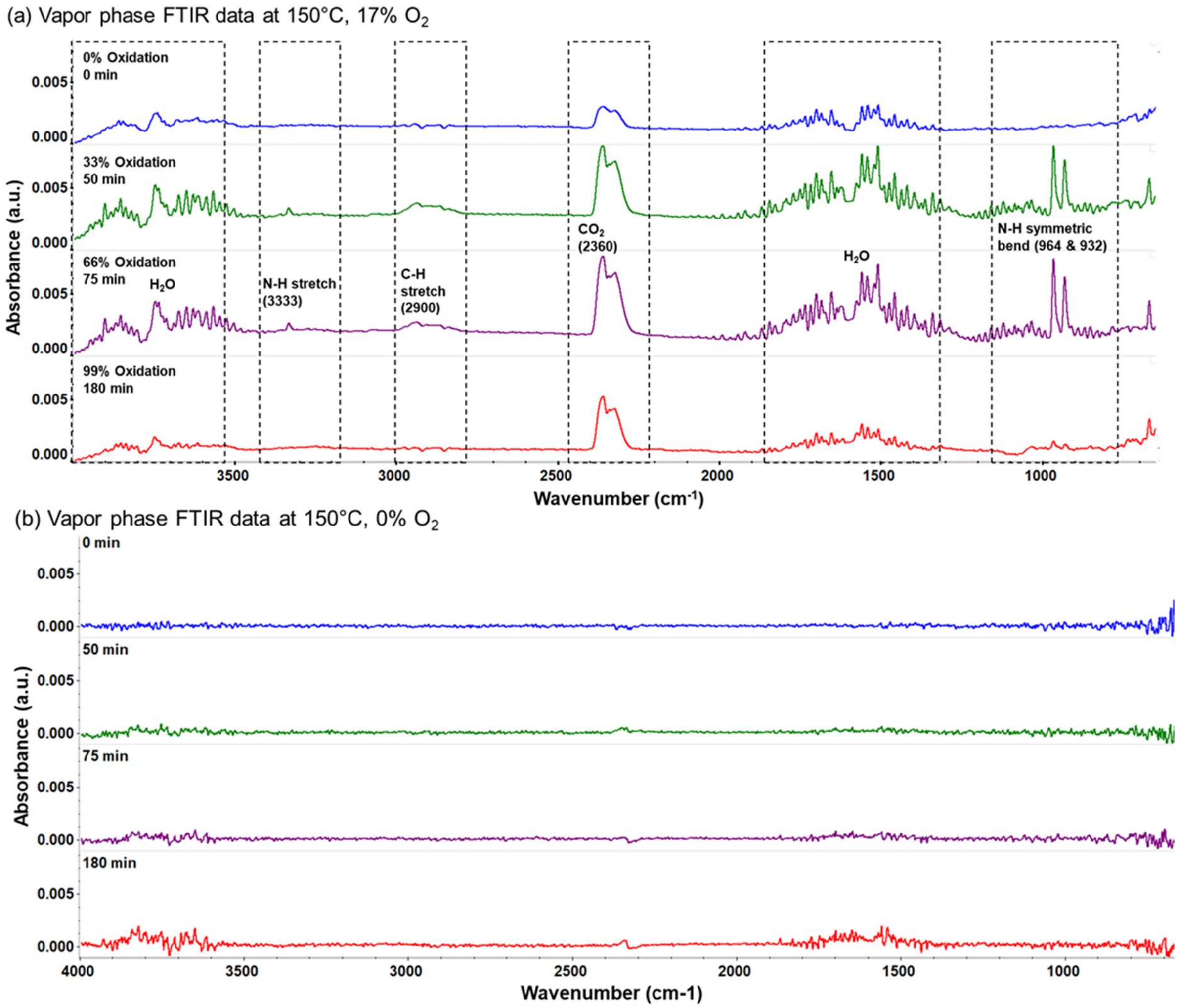


**Figure 1.** FTIR spectra of gaseous reaction effluent with 17% (a) and without (b) $O_2$ at experimental times corresponding to 0% (blue, top), 33% (green, second from top), 66% (purple, second from bottom), and 99% (red, bottom) extent of oxidation at 150 °C.

These spectra show that $NH_3$, $CO_2$, and $H_2O$ are volatile products of the oxidation of PEI and are not formed under purely thermal conditions. $NH_3$ is a known reaction product of the oxidation of MEA and other aqueous amines,[41,54] and was hypothesized as a likely reaction product previously.[40] Additionally, peaks in the C-H stretching region indicate that a C-H containing moiety is evolved, though a full assignment is not possible with the current data. The second important feature from Figure 1 is that over the course of the oxidative reaction, no new peaks are formed and no peaks disappear. This is consistent with a constant set of reactions, rather than a dynamic reaction set that produces different products, occurring over the course of the reaction.

**Formation Rates and Quantities of Volatile Oxidation Products**

The production rates of $NH_3$, $H_2O$, and $CO_2$ formed during the reaction were quantified for further analysis and comparison to the reaction rate. Quantitative values for $NH_3$ were extracted from the FTIR spectra via calibration of the gas cell with known concentrations of $NH_3$ from a cylinder. This allowed the areas of the peaks centered at 964 $cm^{-1}$ and 932 $cm^{-1}$ to be used to estimate the $NH_3$ concentration quantitatively in the gas cell during the experiments. $CO_2$ and $H_2O$ were quantitatively assessed by passing the reaction effluent through a LiCOR 850a analyzer, which is a commercial IR based $CO_2$/$H_2O$ analyzer. Figure 2 shows the molar production profiles of each species normalized per mol of PEI initially present in the sorbent as a function of time at 137.5 °C (Figure 2a), the integral molar production rate of each species as a function of time at 137.5 °C (Figure 2b), the total moles of each species produced at 100% oxidation at each temperature tested (Figure 2c) and the total moles of each species produced at 100% oxidation normalized per mole of primary element present in fresh PEI (Figure 2d). Molar formation rate profiles at 125 °C and 150 °C with 17% $O_2$, and at 150 °C with 0% $O_2$ are shown in Figure S7.

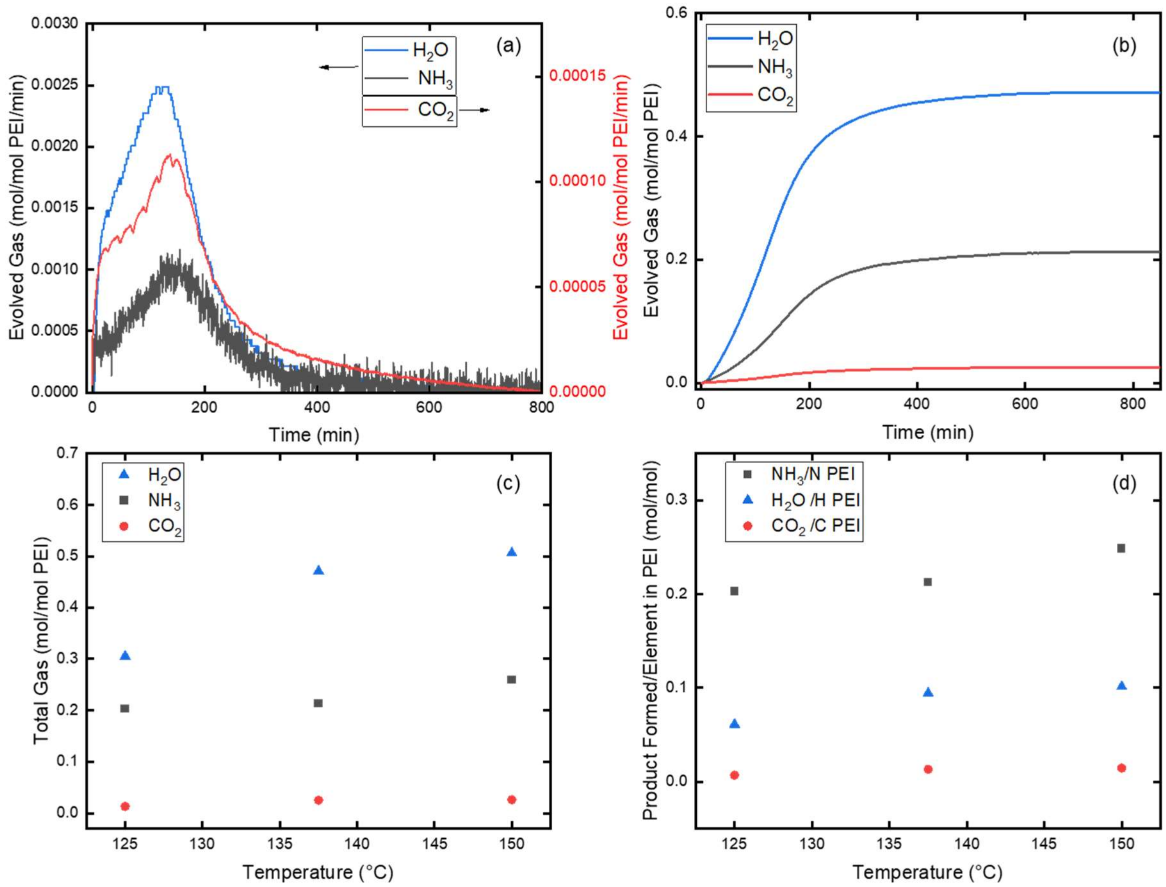


**Figure 2.** Formation rate of $NH_3$, $H_2O$, $CO_2$ during oxidation at 137.5 °C and 17% $O_2$ (a). Total quantity of $NH_3$, $H_2O$, $CO_2$ produced at 137.5 °C and 17% $O_2$ per mol of PEI initially present in the sorbent as a function of time (b). Total quantity of volatile species formed per mole of PEI initially present in the sorbent formed at the end of each oxidation as a function of temperature at 17% $O_2$ (c). Total quantity of volatile species formed per mole of primary element present in PEI ($NH_3$/N, $CO_2$/C, $H_2O$/H) (d).

Figure 2a shows that each gas is produced in a similar production profile: there is an increasing rate of production at early reaction times that eventually peaks and decays as the remaining PEI becomes sparse of additional reaction sites. This is very similar to the shape of the reaction curve as tracked by DSC, as shown previously, and discussed in greater detail below. Figures 2b and 2c show that $H_2O$ forms in the greatest total quantity, followed by $NH_3$ and then finally $CO_2$. The total amount of each gas produced increases with increased temperature, consistent with the total heat evolved as measured by the DSC. Figure 2d shows the amount of each species formed normalized to the quantity of primary element present in PEI (i.e., $NH_3$ normalized to N, $H_2O$ normalized to H, $CO_2$ normalized to C). This shows the relative consumption and conversion of each of the C, H, and N atoms in the PEI molecule to each of the volatile species containing their atoms. These data reveal that 20-25% of the total quantity of amines in PEI are converted to $NH_3$, roughly consistent with the total amount of primary amines present in the fresh PEI,[55] suggesting that $NH_3$ may form from C-N cleavage of these terminal primary amine groups in PEI.

The data also show that ~0.1 mol $H_2O$ is produced per mol H in PEI. Because one mole of $H_2O$ contains two moles of H, this suggests that 20% of H atoms in PEI react to form $H_2O$, corresponding to approximately one H atom per repeat unit of PEI. Our previous work showed that approximately 1.5 H atoms per repeat unit are lost overall. Additional H atoms are also lost from PEI through $NH_3$ formation. The known reaction products of imines and amides both require loss of two H species from the reaction site. Taken together, this suggests that half of the repeat units on the PEI overall may react in dehydration reactions to form imines or amides.

$CO_2$ forms in a minor relative quantity with less than 3% of C in PEI forming $CO_2$; this is expected as $CO_2$ is the result of complete oxidation of a carbon atom, and it is surprising that it forms at all under these mild oxidative conditions.

To compare the formation rates of gaseous species to the overall rate of reaction, the extent of oxidation has been derived from both the DSC data and the rate curves of the gaseous species. Equation 1 below shows how the extent of oxidation is derived from the DSC data, and a full derivation can be found in our previous work. Equation 2 below shows how the extent of oxidation is derived from the FTIR data.

$$\xi(t) = \frac{\int_0^t Q_{DSC}(t)}{\int_0^\infty Q_{DSC}(t)} \qquad (1)$$

Equation 1: Extent of oxidation from DSC

$$\xi(t) = \frac{\int_0^t \dot{n}_{gas}(t)}{\int_0^\infty \dot{n}_{gas}(t)} \qquad (2)$$

Equation 2: Extent of oxidation from $NH_3$ FTIR

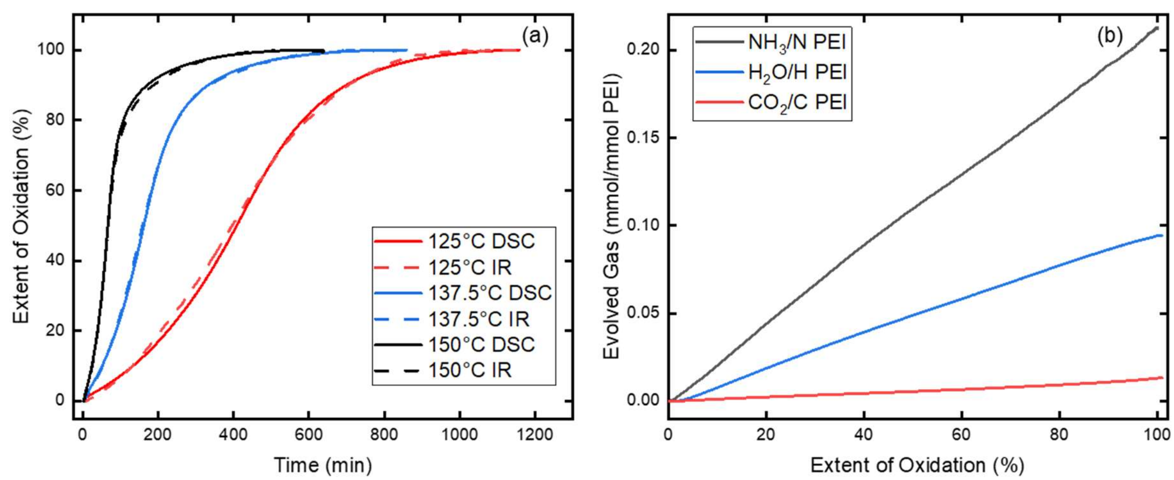


**Figure 3.** Extent of PEI oxidation over time calculated according to Equation 1 using DSC and Equation 2 using molar $NH_3$ flow at 17% $O_2$ and varied temperature (a). Total quantity of volatile species formed per mole of primary element present in PEI ($NH_3$/N, $CO_2$/C, $H_2O$/H) as a function of extent of oxidation calculated from DSC according to Equation 1 (b).

Figure 3a shows the extent of reaction curves estimated from DSC (Eq 1) and from the $NH_3$ FTIR spectra (Eq 2). The data are remarkably consistent, showing that $NH_3$ forms at the same rate as the overall reaction. This finding is both useful and interesting for a variety of reasons. Practically speaking, this means that the rate of $NH_3$ formation can be used as a quantitative proxy for oxidation of PEI, allowing for measurements of oxidation rate to be made *in-situ* during process operation with appropriately selected equipment. This technique is used frequently in the aqueous amine literature.[41] A comparison of the extent of oxidation from the $NH_3$ peak area and DSC heat flow for multiple temperatures and oxygen concentrations is given in Figure S8. Figure 3b shows integral production rates of each of the gaseous species normalized per mol of primary element in PEI, similar to Figure 2d, plotted against the extent of oxidation. When plotted in this fashion, the production profile of each species becomes nearly linear. This means that the same amount of each species is produced along each increment of the oxidation reaction.

**Mol balance around C, H, and N**

In previous work, we showed that the composition of PEI remaining on the sorbent during oxidation systematically changed over the course of the extent of oxidation. In particular, we showed that the C/N ratio of PEI systematically increased and the H/(C+N) ratio systematically decreased. We have furthered this finding here by comparing the measured C/N and H/(C+N) to those predicted by the loss in C, H, and N resulting from the measured quantity of evolved $NH_3$, $H_2O$ and $CO_2$. Figure 4a shows a comparison of measured and predicted C/N and H/(C+N) at 100% oxidation for the 125 °C, 137.5 °C, and 150 °C. Figure 4b shows these predicted (solid lines) and measured (datapoints) C/N and H/(C+N) across the extent of oxidation for the sorbent at 17% $O_2$ and 137.5 °C.

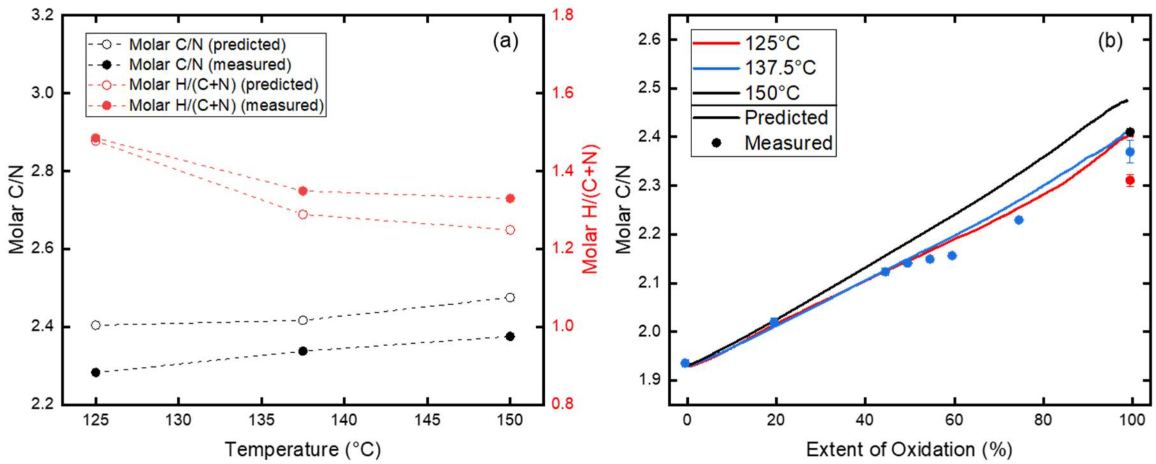


**Figure 4.** Predicted (open datapoints) and measured (closed datapoints) C/N ratios (black, referenced to left axis) and H/(C+N) ratios (red, referenced to right axis) of PEI remaining on the sorbent at 100% oxidation as a function of oxidation temperature (a). Predicted (solid lines) and measured (data points) C/N ratio across the extent of oxidation for the three experimental temperatures probed (b). Predicted molar ratios derived from mole balance of C, H, N as measured by the formation quantities of volatile $NH_3$, $H_2O$, $CO_2$.

Figure 4 shows similar, but imperfect trends in the change in composition of PEI as predicted by the quantities of $NH_3$, $H_2O$, and $CO_2$ formed during the oxidation, and the composition measured directly on the sample following those oxidative treatments. There is a systematic overprediction of C/N and underprediction of H/(C+N) by the moles of volatile species formed; this is likely due to the additional species noted in the FTIR spectra in Figure 1 that contains C-H moieties. Additional carbonaceous species lost in the reaction would cause a lower C/N ratio on the solid sample compared to that predicted when only considering the three gasses probed in this study. Further study will be needed to further probe this hypothesis.

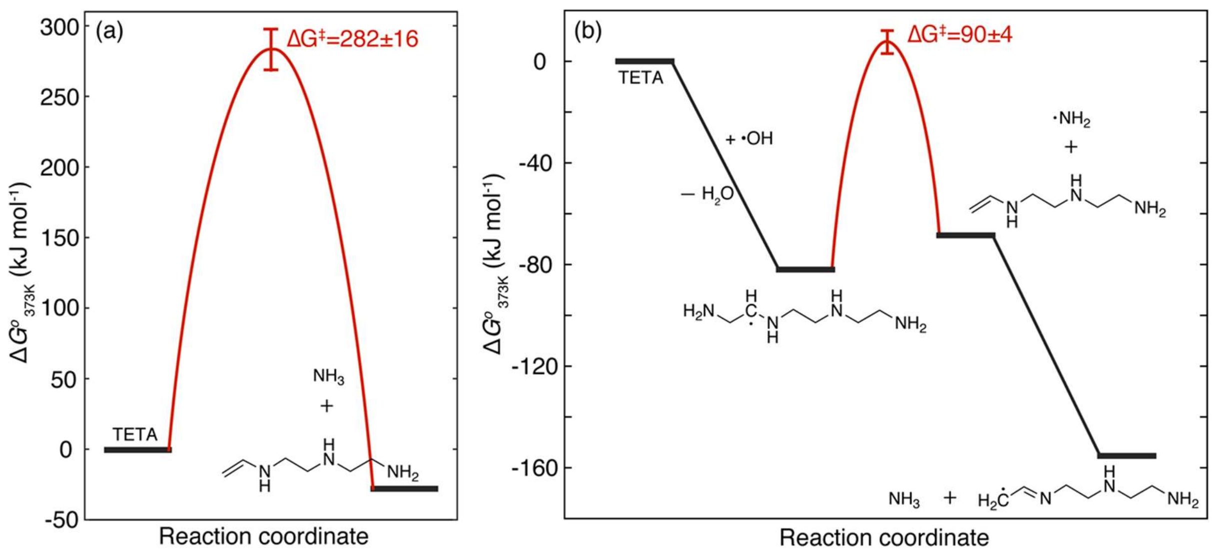


**Figure 5.** Calculated standard state free energy profiles of (a) thermal-driven and (b) radical-facilitated $NH_3$ formation reactions. Structures of reactants, intermediates, and products were optimized with B3LYP functional and energies were further refined with CCSD(t). Free energy barriers of were computed using Metadynamics simulations at PBE+D3 level of theory. Three replicate runs were performed to determine the statistical error bars for each barrier.

**Reaction pathways to form $NH_3$**

To probe possible reaction pathways that may occur on the PEI, metadynamics simulations and CCSD(T) quantum chemical calculations were performed utilizing triethylenetetramine (TETA), a simple linear PEI molecule containing three ethylenimine repeat units. Metadynamics is an *ab initio* molecular dynamics-based advanced free energy sampling method that can provide an effective free energy barrier for a collection of elementary steps that reflect the reaction pathway of interest (e.g. C-N bond breaking). Metadynamics can determine the preferred reaction coordinate with the lowest free energy barrier on the fly, for example choosing between stepwise and concerted bond breaking/forming reaction pathways. Figure 5 shows simulated free energy profiles for potential formation pathways of $NH_3$ from TETA under purely thermal conditions and under oxidative conditions where a free radical is present; representative snapshots near transition states from the metadynamics simulations are shown in Figure S9. Additional discussion about the metadynamics reaction trajectories can be found in the Supporting Information.

The simulations show that in purely thermal conditions (Figure 5a), and in the absence of any radicals, the free energy barrier ($\Delta F_{ACT}$) to forming $NH_3$ is very high ($\Delta F_{ACT}$ ~ 280 kJ/mol), although the overall reaction is exergonic ($\Delta G^{o}_{RXN}$ ~ -28 kJ/mol). This suggests that sluggish dissociation kinetics are likely causing the inert nature of the material in the absence of $O_2$. This is consistent with expectation and the experimental results presented in Figure 1b.

As shown in Figure 5b, however, when a free radical is present, simulated here as a hydroxyl radical which is a common reactive oxygen species, the free energy barrier is substantially reduced to $\Delta F_{ACT}$ ~ 90 kJ/mol. Here, the computed free energy barriers from metadynamics simulations contain both enthalpic and entropic contributions and thus may not correspond quantitatively with the experimentally measured activation energy for $NH_3$ formation. Nonetheless, the computed values are broadly consistent with the experimentally measured overall activation energy of 105 kJ/mol.[40]

In the metadynamics simulated reaction trajectory, a radical is formed on the beta carbon to the terminal amine by a hydroxyl radical abstracting a proton and forming $H_2O$. Naturally, the formation of $H_2O$ in this reaction is consistent with the observations presented above, though it relies on the assumption of a hydroxyl radical[56] being present in the reaction pathway. Hydroxyl radical was chosen for simplicity, due to its prevalence as a reactive oxygen species commonly observed in $O_2$-rich environments, though other species (e.g. OOH radical) with sufficient reactivity could also function as an initiator for alkyl radical formation. However, previous literature has demonstrated distinct degradation kinetics for different aminopolymer backbone structures under the same oxidation conditions,[26] suggesting that the set of free radical generation reactions are unlikely to control the overall rate of oxidation.

The resultant imine is also consistent with previous literature showing that similar non-volatile species form during PEI and TETA oxidation. While the proposed and simulated reaction pathway serves only as one specific example of how radicals can facilitate the C-N bond cleavage and formation of $NH_3$, a detailed enumeration of kinetically plausible reaction pathways is beyond the scope of this work.

These results highlight the likely importance of radicals in the oxidation of PEI, and the complexity of the set of reactions that may be involved in the oxidation mechanism. For instance, oxygen may not directly participate in the elementary reaction that results in the formation of $NH_3$. Like the Basic Autoxidation Scheme[57] wherein a set of reactions are rationalized to oxidize aliphatic polymers and oligomers, oxygen may serve to initiate and propagate a subset of elementary reactions, such as formation of hydroxyl radicals, rather than each one individually. The identification of radicals and intermediates that form in the early stages of the oxidation reaction will be an important research area to further develop these materials.

**Conclusions**

Using TGA-DSC-FTIR we have shown for the first time that $NH_3$, $CO_2$, and $H_2O$ are formed as volatile products during the oxidation of PEI under accelerated conditions. Under the conditions tested, these species account for a majority of the change to the elemental composition of PEI that remains on the sorbent during the oxidation. Each gas forms at a rate that is consistent with the measured overall reaction rate. In particular, the normalized production rate of $NH_3$ predicts the oxidation rate measured by DSC extremely well, demonstrating that it can be used as a proxy to measure oxidation rate in more complex experiments. The total quantity of $NH_3$ formed is consistent with the total amount of primary amines on the PEI (25% of amines), suggesting that this species may form through C-N cleavage of these terminal groups. The total quantity of $H_2O$ formed is consistent with approximately one H per repeat unit of PEI being abstracted in a dehydration reaction to form $H_2O$. Finally, metadynamics and quantum chemical simulations performed on the system demonstrate the likely importance of radicals in the elementary reaction that comprise the oxidative degradation.

**Supporting Information**

Material characterization properties; TGA/DSC-FTIR setup; $NH_3$ calibration curve; FTIR spectra at 125 and 137.5 °C; evolved gas at 125 and 150 °C; extent of oxidation from $NH_3$ peak area and DSC heat flow; representative snapshots of transition state structures.

**Acknowledgements**

This work was supported in part by the U.S. Department of Energy, Office of Science, Basic Energy Sciences, Materials Sciences and Engineering Division. Work at Lawrence Livermore National Laboratory was performed under the auspices of the U.S. Department of Energy under Contract DE-AC52-07NA27344. Computing resources were provided under the LLNL Multiprogrammatic and Institutional Computing Program.

**References**

(1) Sanz-Perez, E. S.; Murdock, C. R.; Didas, S. A.; Jones, C. W. Direct Capture of CO2 from Ambient Air. *Chemical Reviews* **2016**, *116*, 11840–11876. https://doi.org/10.1021/acs.chemrev.6b00173.

(2) Bui, M.; Adjiman, C. S.; Bardow, A.; Anthony, E. J.; Boston, A.; Brown, S.; Fennell, P. S.; Fuss, S.; Galindo, A.; Hackett, L. A., et al. Carbon Capture and Storage (CCS): The Way Forward. *Energy and Environmental Science* **2018**, *11*, 1062–1176. https://doi.org/10.1039/c7ee02342a.

(3) Siegelman, R. L.; Kim, E. J.; Long, J. R. Porous Materials for Carbon Dioxide Separations. *Nature Materials* **2021**, *20*, 1060–1072. https://doi.org/10.1038/s41563-021-01054-8.

(4) Halliday, C.; Hatton, T. A. Sorbents for the Capture of CO2and Other Acid Gases: A Review. *Industrial and Engineering Chemistry Research* **2021**, *60*, 9313–9346. https://doi.org/10.1021/acs.iecr.1c00597.

(5) Shi, X.; Xiao, H.; Azarabadi, H.; Song, J.; Wu, X.; Chen, X.; Lackner, K. S. Sorbents for the Direct Capture of CO2 from Ambient Air. *Angewandte Chemie - International Edition* **2020**, *59*, 6984–7006. https://doi.org/10.1002/anie.201906756.

(6) Xu, X.; Song, C.; Andresen, J. M.; Miller, B. G.; Scaroni, A. W. Novel Polyethylenimine-Modified Mesoporous Molecular Sieve of MCM-41 Type as High-Capacity Adsorbent for CO 2 Capture. *Energy & Fuels* **2002**, *16*, 1463–1469.

(7) Fauth, D. J.; Gray, M. L.; Pennline, H. W.; Krutka, H. M.; Sjostrom, S.; Ault, A. M. Investigation of Porous Silica Supported Mixed-Amine Sorbents for Post-Combustion CO2 Capture. *Energy & Fuels* **2012**, *26*, 2483–2496.

(8) Xu, X.; Song, C.; Miller, B. G.; Scaroni, A. W. Influence of Moisture on CO2 Separation from Gas Mixture by a Nanoporous Adsorbent Based on Polyethylenimine-Modified Molecular Sieve MCM-41. *Ind. Eng. Chem. Res.* **2005**, *44*, 8113–8119.

(9) Goeppert, A.; Czaun, M.; May, R. B.; Prakash, G. K. S.; Olah, G. A.; Narayanan, S. R. Carbon Dioxide Capture from the Air Using a Polyamine Based. *Journal of the American Chemical Society* **2011**, *113*, 20164–20167.

(10) Hicks, J. C.; Drese, J. H.; Fauth, D. J.; Gray, M. L.; Qi, G. G.; Jones, C. W. Designing Adsorbents for CO2 Capture from Flue Gas-Hyperbranched Aminosilicas Capable of Capturing CO2 Reversibly. *Journal of the American Chemical Society* **2008**, *130*, 2902–2903. https://doi.org/Doi 10.1021/Ja077795v.

(11) Sinha, A.; Darunte, L. A.; Jones, C. W.; Realff, M. J.; Kawajiri, Y. Systems Design and Economic Analysis of Direct Air Capture of CO2through Temperature Vacuum Swing Adsorption Using MIL-101(Cr)-PEI-800 and Mmen-Mg2(Dobpdc) MOF Adsorbents. *Industrial and Engineering Chemistry Research* **2017**, *56*, 750–764. https://doi.org/10.1021/acs.iecr.6b03887.

(12) Li, W.; Choi, S.; Drese, J. H.; Hornbostel, M.; Krishnan, G.; Eisenberger, P. M.; Jones, C. W. Steam-Stripping for Regeneration of Supported Amine-Based CO2 Adsorbents. *ChemSusChem* **2010**, *3*, 899–903. https://doi.org/10.1002/cssc.201000131.

(13) Wijesiri, R. P.; Knowles, G. P.; Yeasmin, H.; Hoadley, A. F. A.; Chaffee, A. L. Desorption Process for Capturing CO2 from Air with Supported Amine Sorbent. *Industrial and Engineering Chemistry Research* **2019**, *58*, 15606–15618. https://doi.org/10.1021/acs.iecr.9b03140.

(14) Ebner, A. D.; Gray, M. L.; Chisholm, N. G.; Black, Q. T.; Mumford, D. D.; Nicholson, M. A.; Ritter, J. A. Suitability of a Solid Amine Sorbent for CO 2 Capture by Pressure Swing Adsorption. *Industrial & Engineering Chemistry Research* **2011**, *50*, 5634–5641.

(15) Zhang, W.; Liu, H.; Sun, C.; Drage, T. C.; Snape, C. E. Capturing CO2 from Ambient Air Using a Polyethyleneimine-Silica Adsorbent in Fluidized Beds. *Chemical Engineering Science* **2014**, *116*, 306–316. https://doi.org/10.1016/j.ces.2014.05.018.

(16) Sakwa-Novak, M. A.; Yoo, C. J.; Tan, S.; Rashidi, F.; Jones, C. W. Poly(Ethylenimine)-Functionalized Monolithic Alumina Honeycomb Adsorbents for CO2 Capture from Air. *ChemSusChem* **2016**, *9*, 1859–1868. https://doi.org/10.1002/cssc.201600404.

(17) Fan, Y.; Labreche, Y.; Lively, R. P.; Jones, C. W.; Koros, W. J. Dynamic CO2 Adsorption Performance of Intertnally Cooled Silica-Supported POly(Ethyleneimine) Hollow Fiber Sorbents. *AIChE Journal* **2014**, *60*, 3878–3887. https://doi.org/10.1002/aic.

(18) Calleja, G.; Sanz, R.; Arencibia, A.; Sanz-Pérez, E. S. Influence of Drying Conditions on Amine-Functionalized SBA-15 as Adsorbent of CO2. *Topics in Catalysis* **2011**, *54*, 135–145. https://doi.org/10.1007/s11244-011-9652-7.

(19) Heydari-Gorji, A.; Belmabkhout, Y.; Sayari, A. Degradation of Amine-Supported CO2 Adsorbents in the Presence of Oxygen-Containing Gases. *Microporous and Mesoporous Materials* **2011**, *145*, 146–149. https://doi.org/10.1016/j.micromeso.2011.05.010.

(20) Bollini, P.; Choi, S.; Drese, J. H.; Jones, C. W. Oxidative Degradation of Aminosilica Adsorbents Relevant to Postcombustion CO2 Capture. *Energy & Fuels* **2011**, *25*, 2416–2425.

(21) Jahandar Lashaki, M.; Khiavi, S.; Sayari, A. Stability of Amine-Functionalized CO2 Adsorbents: A Multifaceted Puzzle. *Chemical Society Reviews* **2019**, *48*, 3320–3405. https://doi.org/10.1039/c8cs00877a.

(22) Heydari-Gorji, A.; Sayari, A. Thermal , Oxidative , and CO2 -Induced Degradation of Supported Polyethylenimine Adsorbents. *Industrial & Engineering Chemistry Research* **2012**, *51*, 6887–6894.

(23) Ahmadalinezhad, A.; Sayari, A. Oxidative Degradation of Silica-Supported Polyethylenimine for CO2 Adsorption: Insights into the Nature of Deactivated Species. *Physical Chemistry Chemical Physics : PCCP* **2014**, *16*, 1529–1535. https://doi.org/10.1039/c3cp53928h.

(24) Srikanth, C. S.; Chuang, S. S. C. Infrared Study of Strongly and Weakly Adsorbed CO 2 on Fresh and Oxidatively Degraded Amine Sorbents. *J. Phys. Chem. C* **2013**, *117*, 9196–9205.

(25) Srikanth, C. S.; Chuang, S. S. C. Spectroscopic Investigation into Oxidative Degradation of Silica-Supported Amine Sorbents for CO2 Capture. *ChemSusChem* **2012**, *5*, 1435–1442. https://doi.org/10.1002/cssc.201100662.

(26) Pang, S. H.; Lee, L. C.; Sakwa-Novak, M. A.; Lively, R. P.; Jones, C. W. Design of Aminopolymer Structure to Enhance Performance and Stability of CO2 Sorbents: Poly(Propylenimine) vs Poly(Ethylenimine). *Journal of the American Chemical Society* **2017**, *139*, 3627–3630. https://doi.org/10.1021/jacs.7b00235.

(27) Bali, S.; Chen, T. T.; Chaikittisilp, W.; Jones, C. W. Oxidative Stability of Amino Polymer–Alumina Hybrid Adsorbents for Carbon Dioxide Capture. *Energy & Fuels* **2013**, *27*, 1547–1554. https://doi.org/10.1021/ef4001067.

(28) Yoo, C. J.; Park, S. J.; Jones, C. W. CO2 Adsorption and Oxidative Degradation of Silica-Supported Branched and Linear Aminosilanes. *Industrial and Engineering Chemistry Research* **2020**, *59*, 7061–7071. https://doi.org/10.1021/acs.iecr.9b04205.

(29) Didas, S. A.; Zhu, R.; Brunelli, N. A.; Sholl, D. S.; Jones, C. W. Thermal, Oxidative and CO2 Induced Degradation of Primary Amines Used for CO2 Capture: Effect of Alkyl Linker on Stability. *Journal of Physical Chemistry C* **2014**, *118*, 12302–12311. https://doi.org/10.1021/jp5025137.

(30) Ahmadalinezhad, A.; Tailor, R.; Sayari, A. Molecular-Level Insights into the Oxidative Degradation of Grafted Amines. *Chemistry - A European Journal* **2013**, *19*, 10543–10550. https://doi.org/10.1002/chem.201300864.

(31) Pang, S. H.; Lively, R. P.; Jones, C. W. Oxidatively-Stable Linear Poly(Propylenimine)-Containing Adsorbents for CO2 Capture from Ultradilute Streams. *ChemSusChem* **2018**, *11*, 2628–2637. https://doi.org/10.1002/cssc.201800438.

(32) Chaikittisilp, W.; Khunsupat, R.; Chen, T. T.; Jones, C. W. Poly ( Allylamine ) ÀMesoporous Silica Composite Materials for CO 2 Capture from Simulated Flue Gas or Ambient Air. *Industrial & Engineering Chemistry Research* **2011**, 14203–14210.

(33) Rosu, C.; Pang, S. H.; Sujan, A. R.; Sakwa-Novak, M. A.; Ping, E. W.; Jones, C. W. Effect of Extended Aging and Oxidation on Linear Poly(Propylenimine)-Mesoporous Silica Composites for CO2Capture from Simulated Air and Flue Gas Streams. *ACS Applied Materials and Interfaces* **2020**, *12*, 38085–38097. https://doi.org/10.1021/acsami.0c09554.

(34) Vu, Q. T.; Yamada, H.; Yogo, K. Effects of Amine Structures on Oxidative Degradation of Amine-Functionalized Adsorbents for CO2Capture. *Industrial and Engineering Chemistry Research* **2021**, *60*, 4942–4950. https://doi.org/10.1021/acs.iecr.0c05694.

(35) Min, K.; Choi, W.; Kim, C.; Choi, M. Oxidation-Stable Amine-Containing Adsorbents for Carbon Dioxide Capture. *Nature Communications* **2018**, *9*, 726. https://doi.org/10.1038/s41467-018-03123-0.

(36) Choi, W.; Min, K.; Kim, C.; Ko, Y. S.; Jeon, J. W.; Seo, H.; Park, Y. K.; Choi, M. Epoxide-Functionalization of Polyethyleneimine for Synthesis of Stable Carbon Dioxide Adsorbent in Temperature Swing Adsorption. *Nature Communications* **2016**, *7*, 1–8. https://doi.org/10.1038/ncomms12640.

(37) Kolle, J. M.; Sayari, A. Covalently Immobilized Polyethylenimine for CO2 Adsorption. *Industrial and Engineering Chemistry Research* **2020**, *59*, 6944–6950. https://doi.org/10.1021/acs.iecr.9b04669.

(38) Zhai, Y.; Chuang, S. S. C. Enhancing Degradation Resistance of Polyethylenimine for CO2 Capture with Cross-Linked Poly(Vinyl Alcohol). *Industrial and Engineering Chemistry Research* **2017**, *56*, 13766–13775. https://doi.org/10.1021/acs.iecr.7b03636.

(39) Tanthana, J.; Chuang, S. S. C. In Situ Infrared Study of the Role of PEG in Stabilizing Silica-Supported Amines for CO(2) Capture. *ChemSusChem* **2010**, *3*, 957–964. https://doi.org/10.1002/cssc.201000090.

(40) Nezam, I.; Xie, J.; Golub, K. W.; Carneiro, J.; Olsen, K.; Ping, E. W.; Jones, C. W.; Sakwa-Novak, M. A. Chemical Kinetics of the Autoxidation of Poly(Ethylenimine) in CO2Sorbents. *ACS Sustainable Chemistry and Engineering* **2021**, *9*, 8477–8486. https://doi.org/10.1021/acssuschemeng.1c01367.

(41) Chi, S.; Rochelle, G. T. Oxidative Degradation of Monoethanolamine. *Industrial & Engineering Chemistry Research* **2002**, *41* (17), 4178–4186. https://doi.org/10.1021/ie010697c.

(42) Voice, A. K.; Rochelle, G. T. Oxidation of Amines at Absorber Conditions for CO2 Capture from Flue Gas. *Energy Procedia* **2011**, *4*, 171–178. https://doi.org/10.1016/j.egypro.2011.01.038.

(43) Buvik, V.; Høisæter, K. K.; Vevelstad, S. J.; Knuutila, H. K. A Review of Degradation and Emissions in Post-Combustion CO2 Capture Pilot Plants. *International Journal of Greenhouse Gas Control*. Elsevier Ltd March 1, 2021. https://doi.org/10.1016/j.ijggc.2020.103246.

(44) Kresse, G.; Furthmü, J. Efficient Iterative Schemes for Ab Initio Total-Energy Calculations Using a Plane-Wave Basis Set. *Physical Review B* **1996**, *54*, 11169–11186.

(45) Blochl, P. E. Projector Augmented-Wave Method. *Physical Review B* **1994**, *50*, 17953–17954.

(46) Kresse, G.; Joubert, D. From Ultrasoft Pseudopotentials to the Projector Augmented-Wave Method. *Physical Review B* **1999**, *59*, *1758-1775*.

(47) Perdew, J. P.; Burke, K.; Ernzerhof, M. Generalized Gradient Approximation Made Simple. *Physical Review Letters* **1996**, *77*, 3865–3868.

(48) Becke, A. D. Density-Functional Thermochemistry. III. The Role of Exact Exchange. *The Journal of Chemical Physics* **1993**, *98*, 5648–5652. https://doi.org/10.1063/1.464913.

(49) Stephens, P. J.; Devlin, F. J.; Chabalowski, C. F.; Frisch, M. J. Ab Initio Calculation of Vibrational Absorption and Circular Dichroism Spectra Using Density Functional Force Fields. *The Journal of Physical Chemistry* **1994**, *98*, 11623–11627.

(50) Frisch, M. J.; Trucks, G. W.; Schlegel, H. B.; Scuseria, G. E.; Robb, M. A.; Cheeseman, J. R.; G. Scalmani; Barone,V.; Petersson, G. A.; Nakatsuji, H., et al. *Gaussian 09*, Revision A.02.; Gaussian, Inc.: Wallingford CT.

(51) Aprà, E.; Bylaska, E. J.; de Jong, W. A.; Govind, N.; Kowalski, K.; Straatsma, T. P.; Valiev, M.; van Dam, H. J. J.; Alexeev, Y.; Anchell, J., et al. NWChem: Past, Present, and Future. *Journal of Chemical Physics* **2020**, *152,* 184102. https://doi.org/10.1063/5.0004997.

(52) Laio, A.; Rodriguez-Fortea, A.; Gervasio, F. L.; Ceccarelli, M.; Parrinello, M. Assessing the Accuracy of Metadynamics. *Journal of Physical Chemistry B* **2005**, *109*, 6714–6721. https://doi.org/10.1021/jp045424k.

(53) Li, S.; Zheng, Y.; Gao, F.; Szanyi, J.; Schneider, W. F. Experimental and Computational Interrogation of Fast SCR Mechanism and Active Sites on H-Form SSZ-13. *ACS Catalysis* **2017**, *7*, 5087–5096. https://doi.org/10.1021/acscatal.7b01319.

(54) Sexton, A. J.; Rochelle, G. T. Reaction Products from the Oxidative Degradation of Monoethanolamine. *Industrial and Engineering Chemistry Research* **2011**, *50*, 667–673. https://doi.org/10.1021/ie901053s.

(55) von Harpe, A.; Petersen, H.; Li, Y.; Kissel, T. Characterization of Commercially Available and Synthesized Polyethylenimines for Gene Delivery. *Journal of Controlled Release* **2000**, *69*, 309–322. https://doi.org/10.1016/S0168-3659(00)00317-5.

(56) Møller, K. H.; Berndt, T.; Kjaergaard, H. G. Atmospheric Autoxidation of Amines. *Environmental Science & Technology* **2020**, *54*, 11087–11099. https://doi.org/10.1021/acs.est.0c03937.

(57) Gryn'ova, G.; Hodgson, J. L.; Coote, M. L. Revising the Mechanism of Polymer Autooxidation. *Organic and Biomolecular Chemistry* **2011**, *9*, 480–490. https://doi.org/10.1039/c0ob00596g.